
MGNNI: Multiscale Graph Neural Networks with Implicit Layers

Juncheng Liu Bryan Hooi Kenji Kawaguchi Xiaokui Xiao
National University of Singapore
{juncheng, bhooi, kenji, xiaokui}@comp.nus.edu.sg

Abstract

Recently, implicit graph neural networks (GNNs) have been proposed to capture long-range dependencies in underlying graphs. In this paper, we introduce and justify two weaknesses of implicit GNNs: the constrained expressiveness due to their limited effective range for capturing long-range dependencies, and their lack of ability to capture multiscale information on graphs at multiple resolutions. To show the limited effective range of previous implicit GNNs, we first provide a theoretical analysis and point out the intrinsic relationship between the effective range and the convergence of iterative equations used in these models. To mitigate the mentioned weaknesses, we propose a multiscale graph neural network with implicit layers (MGNNI) which is able to model multiscale structures on graphs and has an expanded effective range for capturing long-range dependencies. We conduct comprehensive experiments for both node classification and graph classification to show that MGNNI outperforms representative baselines and has a better ability for multiscale modeling and capturing of long-range dependencies.

1 Introduction

In recent years, graph neural networks (GNNs) have been widely adopted on graph-related tasks, such as node classification, link prediction, and graph classification [29]. In general, GNNs utilize both node attributes and graph topology to produce meaningful node representations for downstream applications. To achieve this, most modern GNNs follow a “message passing” mechanism: at each iteration, they iteratively aggregate representations of neighboring nodes of each node with its own representation to generate new representations. During this process, each iteration is typically parameterized as a single-layer neural network with learnable weights. Many GNN models have been proposed by adopting different aggregations techniques (e.g., GCN with renormalization [17], GAT with attentive aggregations on neighbors [27], and SGC [28] using aggregations without non-linear activation). In spite of the effectiveness achieved by the aforementioned GNNs on different tasks, they fail to effectively capture long-range information on graphs, since a GNN with T layers can only capture information up to T hops away.

To overcome this deficiency of previous GNNs, recent work has proposed implicit graph neural networks [13, 20, 21] to effectively capture long-range dependencies. These implicit graph neural networks generally define a fixed-point equation as an implicit layer for aggregation and generate the equilibrium Z^* as the node representations. To get the equilibrium, they either use an iterative solver to solve the equation or directly obtain a closed-form solution with guaranteed convergence. Meanwhile, they utilize implicit differentiation to achieve $\mathcal{O}(1)$ memory complexity when computing the gradients during the iterations. As mentioned in Gu et al. [13], Liu et al. [20], these models can be treated as a graph neural network with infinite layers which has the same transformation and shared weights in each layer. This makes them able to effectively capture long-range dependencies without excessive memory requirements as compared with previous GNNs.

Despite the superiority of implicit GNNs shown in several applications requiring long-range information, an important question — what the farthest range these models can capture information from — has not been studied. Although these models are usually claimed as GNNs with infinite depth [13, 20], in this paper, we first point out the *effective range* of these models (i.e., the maximum hops they can effectively capture dependencies for each node) is actually bounded by a certain value. We provide analyses on the intrinsic relationship between the effective range and the convergence of the iterative equation used in implicit GNNs. Specifically, these models usually use a contraction factor γ to ensure the convergence of the iterative map [20, 21], which indeed exponentially decays the distant information during the aggregation at the same time. This design inherently limits the effective range of propagation and hinders their ability to capture long-range dependencies.

Besides the limited effective range, implicit GNNs also cannot effectively capture multiscale information on graphs, i.e., graph features at various scales. In contrast, several GNNs without implicit layers [30, 2, 1, 8] have been proposed to utilize multiscale information to improve the model capacity. For example, Xu et al. [30] proposes JKNet which leverages different neighborhood ranges by skip connections and adaptive aggregations of hidden representations at different layers. MixHop [1] learns neighborhood mixing relationships by mixing hidden representations at various distances. These explicit GNN models demonstrate the effectiveness of utilizing multiscale information from neighbors at various scales. However, it is still not clear how to utilize multiscale information with implicit GNNs since there are no different “layers” in implicit GNNs that can be used for capturing multiscale information at different scales.

Motivated by the above limitations of previous implicit GNNs, we propose our multiscale graph neural network with implicit layers (MGNNI) which brings multiscale modeling into implicit GNNs and expands their effective range for capturing long-range dependencies. We summarize the contributions of this work as follows:

- We introduce the concept of effective range for implicit GNNs, and provide theoretical analyses on the effective range that previous implicit GNNs can capture distant information from. We then point out that their effective range is limited although previous models are generally regarded as GNNs with infinite layers.
- We propose MGNNI as a new implicit GNN model with multiscale propagation to expand the effective range and capture underlying graph information at various scales.
- We conduct comprehensive experiments with synthetic datasets and real-world datasets on both node classification and graph classification to demonstrate that MGNNI has better performance and a better ability to capture both long-range and multiscale information compared with other baselines.

2 Related work

Implicit Models Implicit neural networks use implicit hidden layers which are *implicitly* defined: the outputs are determined by the solutions of some underlying equations. A notable advantage of these implicit models is that they can generally backpropagate through the fixed-point solution using implicit differentiation to achieve *constant* memory complexity regardless of the “depth” of the network. There is an emerging interest in implicit layers in recent years [4, 3, 5, 11]. To name a few, Bai et al. [4] propose the deep equilibrium model (DEQ) demonstrating the ability of implicit models in sequence modeling; Multiscale DEQ (MDEQ) [5] brings multiscale modeling into implicit deep networks for image classification and semantic segmentation. Kawaguchi [15] analyses the global convergence of deep linear implicit models and Geng et al. [11] provide a gradient estimate for implicit models to avoid the costly exact gradient computation.

Graph Neural Networks GNNs have been widely used in different tasks for graph-structured data. Even with different aggregation schemes (e.g., skip connection [30, 8] and attention [27]), convolutional GNNs [17, 28, 30] generally involve finite aggregation layers (usually less than 20 layers) with different learnable weights, which makes them unable to effectively capture long-range dependencies. Although RevGNN [19] is proposed with 1000 layers, it has to use deep reversible architectures [12], which requires excessive amount of time for training. Inspired by implicit models [4, 5] on image and text data, implicit graph neural networks [13, 20, 21] have been proposed to capture long-range information with constant memory complexity. Implicit GNNs generally define an

aggregation equation and obtain the fixed-point solution of the equation as the outputs. In particular, Gu et al. [13] propose IGNN where they ensure the well-posedness and use iterative solvers to obtain fixed-point solutions. Liu et al. [20] propose EIGNN as a linear implicit GNNs where a closed-form solution is derived. Park et al. [21] construct an input-dependent linear iterative map for predicting the properties of a graph system. However, these implicit GNNs cannot model multiscale information in underlying graphs. In contrast, several explicit GNNs, such as JKNet [30], MixHop [1], and N-GCN [2], have shown that multiscale information is helpful to improve the model capability. To fill the gap, our model MGNNI brings multiscale modeling to implicit GNNs.

3 Preliminaries

A graph is represented as $\mathcal{G} = (\mathcal{V}, \mathcal{E})$ which contains the node set \mathcal{V} with n nodes and the edge set \mathcal{E} . In practice, graph neural networks take the adjacency matrix $A \in \mathbb{R}^{n \times n}$ and the node feature matrix $X \in \mathbb{R}^{m \times n}$ of \mathcal{G} as input data. For simplicity, considering unweighted adjacency matrix A , then $A_{i,j} = 1$ if $(i, j) \in \mathcal{E}$, for any two nodes $i, j \in \mathcal{V}$; otherwise $A_{i,j} = 0$. Given input graph data (\mathcal{G}, X) , depending on different classification tasks, graph neural networks are required to provide a prediction \hat{y} for a node or a graph to match the true label y .

Aggregations in GNNs GNNs typically employ a trainable aggregation process that iteratively pass the information from each node to its adjacent nodes, followed by a non-linear activation. Without loss of generality, a typical aggregation step at layer l can be written as follows:

$$Z^{(l+1)} = \phi(W^{(l)}Z^{(l)}S + \Omega^{(l)}X), \quad (1)$$

where $Z^{(l)} \in \mathbb{R}^{h_l \times n}$ is the hidden states in the layer l which stacks the state vectors of every nodes denoted as $z^{(l)} \in \mathbb{R}^{h_l}$; $S \in \mathbb{R}^{n \times n}$ is the normalized adjacency matrix; $W^{(l)} \in \mathbb{R}^{h_{l+1} \times h_l}$ and $\Omega^{(l)} \in \mathbb{R}^{h_{l+1} \times m}$ are the matrices of trainable weight parameters; ϕ denotes a non-linear activation function. Recently proposed GNN models use different forms of this graph aggregation process. For example, simplified graph convolution [28] removes the non-linear activation, use only one weight matrix W , and sets $Z^{(0)} = X$ and $\Omega = 0$.

In addition to GNNs with explicitly defined layers, GNNs with implicit layers [13, 20, 21] also follow a similar aggregation form, but with tied weight matrices W and Ω at each iteration step. For these implicit GNNs, the aggregation step is generally changed to $Z^{(l+1)} = \phi(WZ^{(l)}S + \Omega X)$. Given such an aggregation step, implicit GNNs can be seen as iterating the aggregation step an infinite number of times until convergences. To ensure the convergence, IGNN [13] enforces $\|W\|_\infty \leq \kappa/\lambda_{pf}(A)$ with $\kappa \in [0, 1)$, where λ_{pf} is the Perron-Frobenius (PF) eigenvalue [7]. EIGNN [20] and CGS [21] instead achieve this by introducing a contraction factor γ in the aggregation step.

Using EIGNN as an example, it defines the aggregation as an iterative mapping with a contraction factor γ as follows:

$$Z^{(l+1)} = \gamma g(F)Z^{(l)}S + X, \quad (2)$$

where $\gamma \in [0, 1)$ and $g(W)$ is a bounded mapping that projects the trainable weight matrix F into a Frobenius norm ball of radius < 1 . Given the iterative mapping, implicit GNNs obtain the equilibrium states $Z^* = \phi(WZ^*S + \Omega X)$ as the final representations by using either root-finding approaches or closed-form solutions.

4 Effective range of previous implicit GNNs

Implicit deep learning is considered as a method to increase the effective depth of deep neural networks [4, 24]. Previous works on implicit GNNs (including IGNN [13] and EIGNN [20]) claim that these models can be viewed as an infinite-layer GNN. However, in this section, we point out that the effective range within which previous implicit GNNs can capture the long-range information is actually bounded. In other words, their abilities for capturing long-range dependencies are still restricted. We provide analyses revealing the intrinsic relationship between the effective range and the convergence of the iterative equation in implicit GNNs. In addition, we also provide empirical results to support our analyses.

To investigate the effective range, we first provide an analysis on sensitivity, i.e., how changes in node features of node p affect the equilibrium of a distant node q .

Theorem 1. Given two nodes p and q that are h -hops apart, using Equation (2) for propagation, if we perturb node features $X_{:,p}$ of node p by $\Delta X_{:,p} \in \mathbb{R}^m$, the L2 norm of the change in node q 's equilibrium $\|\Delta Z_{:,q}^*\|$ is upper bounded as follows:

$$\|\Delta Z_{:,q}^*\| \leq \frac{\gamma^h}{1-\gamma} \|g^h(F)\Delta X_{:,p} S_{p,q}^h\|. \quad (3)$$

The complete proof can be found in Appendix A.1.

At first glance, the norm of the change in equilibrium $\|\Delta Z_{:,q}^*\|$ would not be zero no matter how large the distance between node p and q . However, Theorem 1 shows that $\|\Delta Z_{:,q}^*\|$ decays exponentially with distance along the graph. Therefore, in practice, this change will fairly quickly fall below the roundoff error in floating-point numbers or the stopping criterion in the iterative solver used to obtain the fixed-point solution, then the change $\Delta X_{:,p}$ on node p cannot affect the equilibrium of node q . This is the intuition about what we call the effective range. To formalize it, we provide the definition of θ -effective range as follows:

Definition 1. For any given error parameter $\theta > 0$, the θ -effective range h is the maximum integer such that exists some pairs of nodes p and q that are h -hop apart, when node features $X_{:,p}$ of node p are perturbed by $\Delta X_{:,p}$, the L2 norm of the change in node q 's equilibrium $\|\Delta Z_{:,q}^*\| > \theta$.

By Definition 1, we know that, given any $h' > h$, for **all pairs** of node p and q that are h' -hop apart, the L2 norm of the change $\|\Delta Z_{:,q}^*\| \leq \theta$, which means the equilibrium of node q cannot be affected in practice. To analyse the θ -effective range, we can derive the corollary of Theorem 1:

Corollary 1. With Equation (2) for propagation, given any error constant $\theta > 0$, the θ -effective range h is upper bounded: $h < \frac{\ln(\theta(1-\gamma))}{\ln \gamma}$. Therefore, if node features $X_{:,p}$ of node p are perturbed, the perturbation can only affect the equilibrium of nodes which are up to $\frac{\ln(\theta(1-\gamma))}{\ln \gamma}$ -hop away from p .

The complete proof can be found in Appendix A.2. Note that the above analysis is directly applicable to two recent Implicit GNN models with a contraction factor γ , i.e., EIGNN [20] and CGS [21].

Asides from the above analysis, we further verify the theoretical analysis with synthetic experiments on the same chain dataset as in EIGNN [20] and IGNN [13], where the task requires simply passing information from one end to the other of a chain graph. See Appendix C.1 for detailed settings. We use the basic form of EIGNN [20] with iterative methods (i.e., iterating Equation (2) to find the equilibrium) as the model. We follow the same experimental setup in EIGNN and then perturb node features by masking the features of the starting node p to all zeros. To support our theoretical analysis, we investigate how the change of node q 's equilibrium (i.e., $\Delta Z_{:,q}^*$) behaves as q gets farther away from p . In Figure 1, we show that $\|\Delta Z_{:,q}^*\|$ decays as node q gets further from p in terms of the distance. For example, with $\gamma = 0.5$, $\|\Delta Z_{:,q}^*\|$ becomes numerically 0 when q and p are around 25 hops apart, which indicates that node q can no longer receive any information from node p at this distance.

The above theoretical analysis and empirical evidences show how different values of γ can constrain the expressiveness of implicit GNNs, i.e., the range within which they can effectively capture long-range dependencies. In short, smaller γ results in a shorter effective range of implicit GNNs. A straightforward strategy to expand the effective range is to increase γ (e.g., to close to 1). However, a large γ can cause instability and difficulty for the convergence of iterative mapping, which would empirically compromise the efficiency of iterative solvers as found in our experiments. We provide the empirical evidences for this in Appendix B. This raises the question: *how can we capture longer range dependencies while ensuring the convergence of the iterative mapping?* Our multiscale MGNNI approach aims to answer this question.

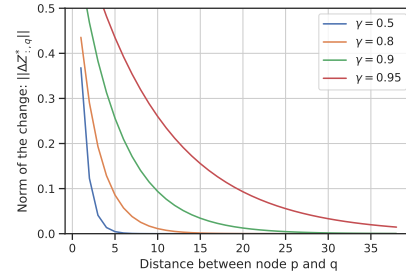


Figure 1: The norm of the change of equilibrium $\|\Delta Z_{:,q}^*\|$ decays as node q becomes further from p .

5 Multiscale implicit graph neural networks

Previous implicit GNNs [13, 20, 21] propagate the information from 1-hop neighbors while applying a decay with the contraction factor γ in each iterative step (e.g., using Equation (2)). As analysed in Section 4, this design inherently limits the effective range of propagation since the information decays exponentially as the range grows linearly. Besides the limited effective range, previous implicit GNNs also cannot capture multiscale information on graphs similarly to explicit GNNs, such as JKNet [30] and MixHop [1], which combine information at different scales of the graph.

Motivated by these limitations, we propose multiscale graph neural networks with implicit layers (MGNNI) which can first expand the effective range to capture long-range dependencies and then capture information from neighbors at various distances. MGNNI contains multiple propagation components with different scales and learns a trainable aggregation mechanism for mixing latent information at various scales.

5.1 The MGNNI model

A single m -scale propagation module in MGNNI model is defined as the following iterative mapping:

$$Z^{(l+1)} = \gamma g(F) Z^{(l)} S^m + f(X, \mathcal{G}), \quad (4)$$

where $\gamma \in [0, 1)$ and m denotes a hyperparameter for the graph scale (i.e., the power of adjacency matrix). $f(X, \mathcal{G})$ is a parameterized transformation on input features and graphs, and $g(F)$ is normalized weight matrix defined as:

$$g(F) = \frac{1}{\|F^\top F\|_F + \epsilon_F} F^\top F \quad (5)$$

with an arbitrary small $\epsilon_F > 0$. Note that in multiscale propagation, at each iterative step, the model can capture the information along with a m -step path, while previous implicit GNNs only consider 1-hop neighbors. In this way, MGNNI is able to capture dependencies within a longer range over iterations. Now we provide the analysis to show that the iterative mapping in MGNNI (i.e., Equation (4)) converges to a unique equilibrium Z^* :

$$\lim_{l \rightarrow \infty} Z^{(l)} = Z^* \quad \text{s.t.} \quad Z^* = \gamma g(F) Z^* S^m + f(X, \mathcal{G}). \quad (6)$$

Theorem 2. *Given the bounded damping factor $\gamma \in [0, 1)$, the proposed iterative map for propagation (i.e., Equation (4)) is a contraction mapping and the unique fixed-point solution Z^* can be obtained by iterating Equation (4).*

This can be proved by using the properties of matrix vectorization and the Kronecker product with the Banach fixed Point Theorem. The complete proof is given in Appendix A.3.

Multiscale propagation With a set of multiple scales $M = \{m_1, \dots, m_k | m_i \neq m_j \forall i, j\}$, we can have multiple propagation modules and obtain k equilibriums with different scales $\{Z^{*1}, Z^{*2}, \dots, Z^{*k}\}$. Given those equilibriums, we propose a scale-aggregation mechanism utilizing learnable attentions, as to learn the contributions of different scales for each node automatically through the learning objective. For each node i , z_i^{*t} denotes t -th equilibrium in Z^{*t} and the attention value β_i^t is defined as follows:

$$\beta_i^t = q^T \tanh(W_a z_i^{*t} + b_a), \quad (7)$$

where q is the parameterized attention weight vector, W_a and b_a are the weight matrix and the bias vector, respectively. Given attention values for different scales $\{\beta^1, \dots, \beta^k\}$, the final weights are normalized by softmax function:

$$\alpha_i^t = \text{softmax}(\beta_i^t) = \frac{\exp(\beta_i^t)}{\sum_{j=1}^k \exp(\beta_i^j)}. \quad (8)$$

Larger α_i^t indicates that the corresponding scale is more important for node i . The final embeddings Z' are obtained by aggregating the equilibriums at different scales with corresponding weights:

$$z'_i = \sum_{t=1}^k \alpha_i^t z_i^{*t}, \quad (9)$$

$$\hat{Y} = f_o(Z'), \quad (10)$$

where the predictions \hat{Y} are generated by a problem-specific decoding function f_o .

5.2 Expanded range via multiscale propagation

In multiscale propagation, nodes receive information from further m -hop neighbors rather than only immediate neighbors, which enlarges the effective range of message passing. It is similar with a larger receptive field in convolutional neural networks. We prove that the effective range for receiving distant information is enlarged by using multiscale propagation.

Theorem 3. *Given two nodes p and q are h -hop apart, using propagation with m -hop neighbors (i.e., Equation (4)), if we perturb node features $X_{:,p}$ of node p by $\Delta X_{:,p} \in \mathbb{R}^m$, the L2 norm of the change in node q 's equilibrium $\|\Delta Z_{:,q}^*\|$ is upper bounded as follows:*

$$\|\Delta Z_{:,q}^*\| \leq \frac{\gamma^{\frac{h}{m}}}{1-\gamma} \|g^{\frac{h}{m}}(F)\Delta X_{:,p} S_{p,q}^h\|. \quad (11)$$

The complete proof is provided in Appendix A.5.

Similar to Corollary 1, we analyse the effective range of multiscale propagation by considering when the change in the equilibrium of node q becomes smaller than a certain numerical error.

Corollary 2. *Using propagation with m -hop neighbors (i.e., Equation (4)), given any small error constant θ , the θ -effective range $h < \frac{m \ln(\theta(1-\gamma))}{\ln \gamma}$. Hence, the perturbation on node features of node p can affect the equilibrium of nodes which are located up to $\frac{m \ln(\theta(1-\gamma))}{\ln \gamma}$ -hop away from p .*

This is the corollary of Theorem 3. The proof is given in Appendix A.5. Under the same condition, the effective range is expanded by using multiscale propagation to consider m -hop neighbors in a propagation step.

5.3 Training MGNNI

To train MGNNI, we can simply iterate Equation (4) until it converges to the equilibrium Z^* for the forward pass. We do not use closed-form solutions as in Liu et al. [20] since it would slow the training with large graphs and a large number of node features. For backward pass, given a loss ℓ , we can use implicit differentiation to compute the gradients of trainable parameters by directly differentiating through the equilibrium Z^* by:

$$\frac{\partial \ell}{\partial (\cdot)} = \frac{\partial \ell}{\partial Z^*} (I - J_\varphi(Z^*))^{-1} \frac{\partial \varphi(Z^*, X, \mathcal{G})}{\partial (\cdot)}, \quad (12)$$

where $Z^* = \varphi(Z^*, X, \mathcal{G}) = \gamma g(F)Z^* S^m + f(X, \mathcal{G})$ and $J_\varphi(Z^*) = \frac{\partial \varphi(Z^*, X, \mathcal{G})}{\partial Z^*}$. We provide the complete derivation in Appendix A.6. One of advantages of directly differentiating through Z^* is that the memory consumption is only one layer regardless the number of iterative steps in forward pass. In contrast, differentiating over iterative steps requires large memory to store intermediate variables.

Note that $(I - J_\varphi(Z^*))^{-1}$ in Equation 12 is expensive to compute due to the computation of the Jacobian $J_\varphi(Z^*)$ and the inverse. However, we can solve a linear equation with a Vector-Jacobian product (VJP) to achieve cheaper computation of $\frac{\partial \ell}{\partial Z^*} (I - J_\varphi(Z^*))^{-1}$:

$$u^T = u^T J_\varphi(Z^*) + \frac{\partial \ell}{\partial Z^*}. \quad (13)$$

Note that, the VJP $u^T J_\varphi(Z^*)$ can be efficiently computed by automatic differentiation packages (e.g., PyTorch [22]) without forming the Jacobian. Subsequently, the gradients $\frac{\partial \ell}{\partial (\cdot)}$ can be obtained.

5.4 Discussion and comparison with previous implicit GNNs

In general, compared to previous implicit GNNs (i.e., IGNN [13], EIGNN [20], and CGS [21]), our model MGNNI brings multiscale modeling to implicit GNNs, which allows the model to capture graph information of different granularities. The multiscale idea has shown its effectiveness on explicit GNN models, such as N-GCN [2], JKNet [30], and MixHop [1]. However, to our knowledge, there is no previous implicit GNNs able to capture graph information at various scales. Specifically, MGNNI essentially has multiple implicit layers with different focuses on various scales coexisting side by side.

Computational complexity MGNNI has similar time complexity with IGNN and CGS as they all use iterative methods to iterate Equation (4) until convergence. The asymptotic time complexity is $O(K(h^2n + hn^2))$ where h is the number of hidden units after the input transformation $f(X, \mathcal{G})$ and K is the number of iterations in an iterative method. In contrast, EIGNN costs $O(n^3)$ to conduct eigendecomposition for the adjacency S , which is costly and prohibitive for large graphs. Additionally, for training, it requires $O(h_i^3 + h_i^2n)$ to get the closed-form solution and $O(h_i^3)$ to conduct eigendecomposition for the weights, where h_i is the number of input features. Comparing MGNNI and EIGNN, MGNNI is more efficient on large graphs as it utilizes iterative solvers for fixed-point solutions, whereas EIGNN requires eigendecomposition to get closed-form solutions.

The above analysis of computational complexity mainly considers the process of propagation. Here, we discuss the time complexity of some additional operations in these implicit GNNs, e.g., the attention mechanism in MGNNI and the projection on the weight matrix in IGNN, which generally cost much less time compared with the main propagation process. The attention mechanism used in MGNNI has the time complexity $O(h'hn + hn)$ (according to Equation 7), where h' is the number of hidden units in the attention module. Similarly, IGNN also has some additional operations, e.g., it requires a projection of the weight matrix W in each training iteration to ensure the well-posedness condition $\|W\|_\infty \leq \kappa/\lambda_{\text{pf}}(A)$. It needs $O(n^2)$ to get and modify the maximum row sum of W (i.e., $\|W\|_\infty$). Overall, MGNNI has the same level of time complexity compared with IGNN and CGS.

6 Experiments

In this section, we show that MGNNI can effectively capture long-range dependencies and mixed graph information at various scales. Therefore, MGNNI provides better performance on both node classification and graph classification compared with representative baselines. Specifically, we conduct the experiments¹ on 7 datasets for node classification (including 1 synthetic and 6 real-world datasets: Color-counting, Cornell, Texas, Wisconsin, Chameleon, Squirrel, PPI) and 6 datasets (MUTAG, PTC, PROTEINS, NCI1, IMDB-Binary, IMDB-Multi) for graph classification. As we follow the same experimental settings on some datasets, we reuse the results of some baselines from literatures. Descriptions of datasets and experimental settings are detailed in Appendix C.

6.1 Experiments with synthetic datasets

Color-counting dataset We construct the synthetic dataset for node classification. The graph contains several chains and some nodes on each chain have different colors. The color information is encoded in node features. The nodes on the same chain share the same label which is the majority color appeared on this chain. The model is supposed to predict the majority color on a chain, which requires the model able to capture the long-range dependencies and also count the occurrence of each color. In Figure 2, we compare MGNNI with different scales against previous implicit GNN models (i.e., IGNN, EIGNN, and CGS). MGNNI ($M=\{1,4,8\}$) denotes that three scales with $m=1$, $m=4$, and $m=8$ are used. MGNNI with higher exponents (i.e., $M=\{1,4,8\}$) generally performs better than IGNN and CGS, which indicates that multiscale propagation with higher-hop neighbors can effectively expand the effective range for long-range dependencies. Note that MGNNI ($M=\{1\}$) can be regarded as MGNNI with only single scale. It is outperformed by MGNNI ($M=\{1,4,8\}$), which again shows the effectiveness of multiscale propagation. MGNNI ($M=\{1\}$), IGNN and CGS are all outperformed by EIGNN, suggesting that implicit GNNs with iterative solvers may still suffer from approximation error issues. We also provide the comparison between MGNNI and representative explicit GNNs in Appendix C.1 (See Figure 5). It further demonstrates the superiority of MGNNI over explicit GNNs in terms of the ability of capturing long-range dependencies.

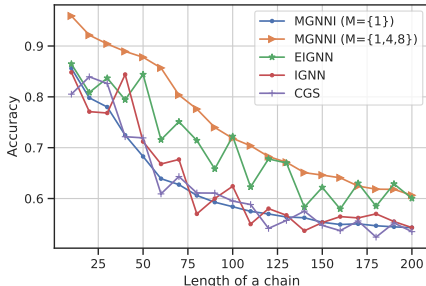


Figure 2: Averaged accuracies on color-counting dataset.

¹The implementation can be found at <https://github.com/liu-jc/MGNNI>

Table 1: Results on heterophilic graph datasets: mean accuracy (%) \pm stdev over different data splits.

	Cornell	Texas	Wisconsin	Chameleon	Squirrel
# Nodes	183	183	251	2,277	5,201
# Edges	280	295	466	31,421	198,493
# Classes	5	5	5	5	5
Geom-GCN [23]	60.81	67.57	64.12	60.90	38.14
SGC [28]	58.91 \pm 3.15	58.92 \pm 4.32	59.41 \pm 6.39	40.63 \pm 2.35	28.4 \pm 1.43
GCN [17]	59.19 \pm 3.51	64.05 \pm 5.28	61.17 \pm 4.71	42.34 \pm 2.77	29.0 \pm 1.10
GAT [27]	59.46 \pm 6.94	61.62 \pm 5.77	60.78 \pm 8.27	46.03 \pm 2.51	30.51 \pm 1.28
APPNP [18]	63.78 \pm 5.43	64.32 \pm 7.03	61.57 \pm 3.31	43.85 \pm 2.43	30.67 \pm 1.06
JKNet [30]	58.18 \pm 3.87	63.78 \pm 6.30	60.98 \pm 2.97	44.45 \pm 3.17	30.83 \pm 1.65
GCNII [8]	76.75 \pm 5.95	73.51 \pm 9.95	78.82 \pm 5.74	48.59 \pm 1.88	32.20 \pm 1.06
H2GCN [34]	82.22 \pm 5.67	84.76 \pm 5.57	85.88 \pm 4.58	60.30 \pm 2.31	40.75 \pm 1.44
IGNN [13]	61.35 \pm 4.84	58.37 \pm 5.82	53.53 \pm 6.49	41.38 \pm 2.53	24.99 \pm 2.11
EIGNN [20]	85.13 \pm 5.57	84.60 \pm 5.41	86.86 \pm 5.54	62.92 \pm 1.59	46.37 \pm 1.39
CGS [21]	68.11 \pm 9.41	62.97 \pm 9.23	63.53 \pm 9.81	40.57 \pm 1.61	31.78 \pm 0.89
MGNNI	85.95 \pm 6.10	84.86 \pm 5.91	86.67 \pm 4.31	63.93 \pm 2.21	54.50 \pm 2.10

Besides the experiments on Color-counting dataset, following Liu et al. [20], we also conduct synthetic experiments on Chains dataset. MGNNI and EIGNN both maintain 100% test accuracy, demonstrating the advantages of capturing long-range dependencies. The results and detailed analyses can be found in Appendix C.1 and Figure 4.

6.2 Experiments with real-world datasets

Node classification Apart from the synthetic experiments, following Pei et al. [23], we also conduct experiments on 5 heterophilic datasets (Cornell, Texas, Wisconsin, Chameleon, and Squirrel) for node classification. On heterophilic graphs, the nodes with different class labels tend to be connected, which requires models to aggregate information from distant nodes. These graph datasets are web-page graphs of the corresponding universities or the corresponding Wikipedia pages. We use the standard train/test/val splits as in Pei et al. [23]. See the detailed setting in Appendix C.2.

The results are shown in Table 1. MGNNI generally achieves the best performance on most datasets. Comparing MGNNI and EIGNN, MGNNI provides better results, especially on Chameleon and Squirrel, which indicates that MGNNI has the superior ability of capturing long-range dependencies and multiscale information. Among implicit GNN baselines, EIGNN outperforms IGNN and CGS, which might be attributed to the less approximation error in the closed-form solution of EIGNN. Among explicit GNN baselines, H2GCN and GCNII are usually better than others, suggesting that the aggregation design in H2GCN and deeper models with residual connections are helpful on heterophilic graphs.

In addition, we also evaluate MGNNI on Protein-Protein Interaction (PPI) dataset which have multiple graphs. On each graph, proteins are presented as nodes and edges are formed if there is an interaction between two proteins. The task is to predict node labels on multi-label multi-graph inductive setting. The same train/val/test split are used as in Hamilton et al. [14]. Table 2 reports the micro-F1 scores of MGNNI against other baseline models. Compared to IGNN and EIGNN, MGNNI achieves 1.1% and 0.7% absolute improvement respectively by effectively capturing underlying multiscale information and long-range dependencies between proteins. Unlike IGNN having 4 implicit layers sequentially stacked, on PPI dataset, MGNNI resorts to parallel equilibrium layers with different scales, which makes MGNNI more efficient than IGNN. We report the efficiency comparison between MGNNI and other implicit GNNs in Appendix C.4.

Table 2: Multi-label node classification on PPI: Micro-F1 (%).

Method	Micro-F1
GCN [17]	59.2
GraphSAGE [14]	78.6
SSE [9]	83.6
GAT [27]	97.3
JKNet [30]	97.6
IGNN [13]	97.6
EIGNN [20]	98.0
MGNNI	98.7

Table 3: Mean accuracy (%) \pm stdev over 10 folds on real-world datasets for graph classification.

	MUTAG	PTC	PROTEINS	NCI	IMDB-B	IMDB-M
# Graphs	188	344	1113	4110	1000	1500
Avg # Nodes	17.9	25.5	39.1	29.8	19.8	13.0
# Classes	2	2	2	2	2	3
GCN [17]	85.6 \pm 5.8	64.2 \pm 4.3	76.0 \pm 3.2	80.2 \pm 2.0	-	-
GIN [31]	89.0 \pm 6.0	63.7 \pm 8.2	75.9 \pm 3.8	82.7 \pm 1.6	75.1 \pm 5.1	52.3 \pm 2.8
DGCNN [33]	85.8	58.6	75.5	74.4	70.0	47.8
FDGNN [10]	88.5 \pm 3.8	63.4 \pm 5.4	76.8 \pm 2.9	77.8 \pm 1.6	72.4 \pm 3.6	50.0 \pm 1.3
IGNN [13]	89.3 \pm 6.7	70.1 \pm 5.6	77.7 \pm 3.4	80.5 \pm 1.9	-	-
EIGNN [20]	88.9 \pm 1.1	69.8 \pm 5.3	75.9 \pm 6.4	77.5 \pm 2.2	72.3 \pm 4.3	52.1 \pm 2.9
CGS [21]	89.4 \pm 5.6	64.7 \pm 6.4	76.3 \pm 6.3	77.2 \pm 2.0	73.1 \pm 3.3	51.1 \pm 2.2
MGNNI	91.9 \pm 5.5	72.1 \pm 2.8	79.2 \pm 2.9	78.9 \pm 2.1	75.8 \pm 3.4	53.5 \pm 2.8

Graph classification Besides node classification, we conduct experiments on graph classification tasks, using four bioinformatics datasets (MUTAG, PTC, PROTEINS, NCI) [32] and two social-network datasets (IMDB-Binary and IMDB-Multi). 10-fold Cross-validation is conducted as [31] and the averaged accuracies with standard deviations are reported in Table 3. The results of baselines are borrowed from Gu et al. [13] and Park et al. [21]. In general, compared with other implicit and explicit baseline models, MGNNI achieves the best performance on 3 out of 4 bioinformatics datasets and both two social-network datasets. This shows that the ability to capture long-range dependencies and multiscale information is helpful for graph classification and can be generalized to test graphs in the inductive setting.

6.3 Ablation Study

To further investigate the effectiveness of multiscale modeling and the contributions of different scales, we conduct the ablation study using different MGNNI variants with various scale combinations. As shown in Table 4, compared to variants with a single scale (i.e., {1}, {2} and {3}), multiscale variants generally achieve better performance on all three datasets. This verifies that multiscale modeling is effective and plays an important role in capturing graph information at various scales. Comparing variants with a single scale, the variant utilizing 1-hop propagation performs best on PPI and Chameleon, whereas the variant with only 3-hop propagation obtains the best performance on Texas. This demonstrates that information at a certain scale can be more important than others on graphs with different properties. Merely considering 1-hop propagation as in previous implicit GNNs might lead to sub-optimal performance.

Table 4: Performance of different scales.

Scales	PPI	Chameleon	Texas
{1}	98.35	61.46	81.35
{2}	94.62	58.24	82.97
{3}	88.56	56.07	83.78
{1,2}	98.67	63.93	83.24
{1,2,3}	98.74	63.75	84.86

Besides the overall performance of different variants, in Figure 3, we also demonstrate the attention values of 100 randomly sampled nodes using MGNNI with scales {1, 2, 3} on PPI and Chameleon. Most of the nodes on chameleon tend to have high attention weights on the first scale and rarely have attentions on the third scale, whereas some nodes on PPI have relatively higher attention values on the third scale than on the first scale. Moreover, compared to Chameleon, there are more nodes on PPI prefer the second and the third scale. These phenomena verify the effectiveness of the attention module in MGNNI, and show that different nodes might prefer information at different scales according to the graph property. Additionally, we also conduct the ablation study on the effect of the attention mechanism in MGNNI (see Appendix C.5).

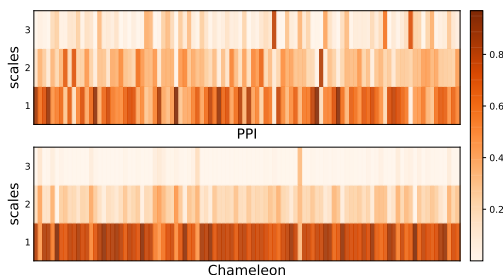


Figure 3: Attention weights of nodes at different scales on PPI and Chameleon.

7 Conclusion

In this paper, we provide theoretical analyses on the constrained expressiveness of previous implicit GNNs due to the limited effective range for capturing distant information. We propose MGNNI which has an expanded effective range and the ability to learn mixing graph information at various scales. With synthetic experiments, we show that MGNNI with a large effective range has a better capacity to capture long-range dependencies. On various real-world datasets for both node classification and graph classification, MGNNI demonstrates superior performances compared with representative baselines, showing the effectiveness of multiscale modeling. Furthermore, the ablation study also shows that MGNNI allows different nodes to have different scale preferences, which plays an important role in adaptively capturing graph information at various scales.

Although MGNNI has the advantages of capturing multiscale graph information, MGNNI also has the limitation on potential approximation errors introduced in the iterative method as IGNN and CGS. EIGNN gets rid of these errors by using a closed-form solution with eigendecomposition which prohibits its usage on large graphs. How to mitigate approximation errors while ensuring the scalability on large graphs could be an interesting topic for future work.

Acknowledgments and Disclosure of Funding

We would like to gratefully thank the insightful feedback and suggestions from the anonymous reviewers. We also appreciate their engagement during the discussion period. This work was supported by Proximate Beta (Grant No. A-8000177-00-00). The views and conclusions contained in this paper are those of the authors and should not be interpreted as representing any funding agencies.

References

- [1] Sami Abu-El-Haija, Bryan Perozzi, Amol Kapoor, Nazanin Alipourfard, Kristina Lerman, Hrayr Harutyunyan, Greg Ver Steeg, and Aram Galstyan. MixHop: Higher-order graph convolutional architectures via sparsified neighborhood mixing. In *Proceedings of the 36th International Conference on Machine Learning*, 2019.
- [2] Sami Abu-El-Haija, Amol Kapoor, Bryan Perozzi, and Joonseok Lee. N-gcn: Multi-scale graph convolution for semi-supervised node classification. In *Proceedings of The 35th Uncertainty in Artificial Intelligence Conference*, 2020.
- [3] Brandon Amos and J Zico Kolter. Optnet: Differentiable optimization as a layer in neural networks. In *International Conference on Machine Learning*, 2017.
- [4] Shaojie Bai, J. Zico Kolter, and Vladlen Koltun. Deep equilibrium models. In *Advances in Neural Information Processing Systems*, 2019.
- [5] Shaojie Bai, Vladlen Koltun, and J. Zico Kolter. Multiscale deep equilibrium models. In *Advances in Neural Information Processing Systems*, 2020.
- [6] Peter W Battaglia, Jessica B Hamrick, Victor Bapst, Alvaro Sanchez-Gonzalez, Vinicius Zambaldi, Mateusz Malinowski, Andrea Tacchetti, David Raposo, Adam Santoro, Ryan Faulkner, et al. Relational inductive biases, deep learning, and graph networks. *arXiv preprint arXiv:1806.01261*, 2018.
- [7] Abraham Berman and Robert J Plemmons. *Nonnegative matrices in the mathematical sciences*. SIAM, 1994.
- [8] Ming Chen, Zhewei Wei, Zengfeng Huang, Bolin Ding, and Yaliang Li. Simple and deep graph convolutional networks. In *International Conference on Machine Learning*, 2020.
- [9] Hanjun Dai, Zornitsa Kozareva, Bo Dai, Alex Smola, and Le Song. Learning steady-states of iterative algorithms over graphs. In *Proceedings of the 35th International Conference on Machine Learning*, 2018.
- [10] Claudio Gallicchio and Alessio Micheli. Fast and deep graph neural networks. In *Proceedings of the AAAI conference on artificial intelligence*, 2020.

- [11] Zhengyang Geng, Xin-Yu Zhang, Shaojie Bai, Yisen Wang, and Zhouchen Lin. On training implicit models. In *Advances in Neural Information Processing Systems*, 2021.
- [12] Aidan N Gomez, Mengye Ren, Raquel Urtasun, and Roger B Grosse. The reversible residual network: Backpropagation without storing activations. 2017.
- [13] Fangda Gu, Heng Chang, Wenwu Zhu, Somayeh Sojoudi, and Laurent El Ghaoui. Implicit graph neural networks. In *Advances in Neural Information Processing Systems*, 2020.
- [14] Will Hamilton, Zhitao Ying, and Jure Leskovec. Inductive representation learning on large graphs. In *Advances in Neural Information Processing Systems*, 2017.
- [15] Kenji Kawaguchi. On the theory of implicit deep learning: Global convergence with implicit layers. In *International Conference on Learning Representations (ICLR)*, 2021.
- [16] Diederick P Kingma and Jimmy Ba. Adam: A method for stochastic optimization. In *International Conference on Learning Representations (ICLR)*, 2015.
- [17] Thomas N Kipf and Max Welling. Semi-supervised classification with graph convolutional networks. In *International Conference on Learning Representations*, 2016.
- [18] Johannes Klicpera, Aleksandar Bojchevski, and Stephan Günnemann. Predict then propagate: Graph neural networks meet personalized pagerank. In *International Conference on Learning Representations*, 2018.
- [19] Guohao Li, Matthias Müller, Bernard Ghanem, and Vladlen Koltun. Training graph neural networks with 1000 layers. In *International conference on machine learning*, 2021.
- [20] Juncheng Liu, Kenji Kawaguchi, Bryan Hooi, Yiwei Wang, and Xiaokui Xiao. Eignn: Efficient infinite-depth graph neural networks. In *Advances in Neural Information Processing Systems*, 2021.
- [21] Junyoung Park, Jinhyun Choo, and Jinkyoo Park. Convergent graph solvers. In *International Conference on Learning Representations*, 2022.
- [22] Adam Paszke, Sam Gross, Francisco Massa, Adam Lerer, James Bradbury, Gregory Chanan, Trevor Killeen, Zeming Lin, Natalia Gimelshein, Luca Antiga, Alban Desmaison, Andreas Kopf, Edward Yang, Zachary DeVito, Martin Raison, Alykhan Tejani, Sasank Chilamkurthy, Benoit Steiner, Lu Fang, Junjie Bai, and Soumith Chintala. Pytorch: An imperative style, high-performance deep learning library. In *Advances in Neural Information Processing Systems*, 2019.
- [23] Hongbin Pei, Bingzhe Wei, Kevin Chen-Chuan Chang, Yu Lei, and Bo Yang. Geom-gcn: Geometric graph convolutional networks. In *International Conference on Learning Representations*, 2020.
- [24] Zaccharie Ramzi, Florian Mannel, Shaojie Bai, Jean-Luc Starck, Philippe Ciuciu, and Thomas Moreau. SHINE: SHaring the INverse estimate from the forward pass for bi-level optimization and implicit models. In *International Conference on Learning Representations*, 2022.
- [25] Benedek Rozemberczki, Carl Allen, and Rik Sarkar. Multi-Scale Attributed Node Embedding. *Journal of Complex Networks*, 2021.
- [26] Aravind Subramanian, Pablo Tamayo, Vamsi K Mootha, Sayan Mukherjee, Benjamin L Ebert, Michael A Gillette, Amanda Paulovich, Scott L Pomeroy, Todd R Golub, Eric S Lander, et al. Gene set enrichment analysis: a knowledge-based approach for interpreting genome-wide expression profiles. *Proceedings of the National Academy of Sciences*, 2005.
- [27] Petar Veličković, Guillem Cucurull, Arantxa Casanova, Adriana Romero, Pietro Liò, and Yoshua Bengio. Graph Attention Networks. In *International Conference on Learning Representations*, 2018.
- [28] Felix Wu, Amauri Souza, Tianyi Zhang, Christopher Fifty, Tao Yu, and Kilian Weinberger. Simplifying graph convolutional networks. In *Proceedings of the 36th International Conference on Machine Learning*, 2019.

- [29] Zonghan Wu, Shirui Pan, Fengwen Chen, Guodong Long, Chengqi Zhang, and S Yu Philip. A comprehensive survey on graph neural networks. *IEEE transactions on neural networks and learning systems*, 2020.
- [30] Keyulu Xu, Chengtao Li, Yonglong Tian, Tomohiro Sonobe, Ken-ichi Kawarabayashi, and Stefanie Jegelka. Representation learning on graphs with jumping knowledge networks. In *International Conference on Machine Learning*, 2018.
- [31] Keyulu Xu, Weihua Hu, Jure Leskovec, and Stefanie Jegelka. How powerful are graph neural networks? In *International Conference on Learning Representations*, 2019.
- [32] Pinar Yanardag and SVN Vishwanathan. Deep graph kernels. In *Proceedings of the 21th ACM SIGKDD international conference on knowledge discovery and data mining*, 2015.
- [33] Muhan Zhang, Zhicheng Cui, Marion Neumann, and Yixin Chen. An end-to-end deep learning architecture for graph classification. In *Thirty-second AAAI conference on artificial intelligence*, 2018.
- [34] Jiong Zhu, Yujun Yan, Lingxiao Zhao, Mark Heimann, Leman Akoglu, and Danai Koutra. Beyond homophily in graph neural networks: Current limitations and effective designs. In *Advances in Neural Information Processing Systems*, 2020.

Checklist

1. For all authors...
 - (a) Do the main claims made in the abstract and introduction accurately reflect the paper's contributions and scope? [Yes]
 - (b) Did you describe the limitations of your work? [Yes] We discuss the limitations in our conclusion.
 - (c) Did you discuss any potential negative societal impacts of your work? [N/A]
 - (d) Have you read the ethics review guidelines and ensured that your paper conforms to them? [Yes]
2. If you are including theoretical results...
 - (a) Did you state the full set of assumptions of all theoretical results? [Yes]
 - (b) Did you include complete proofs of all theoretical results? [Yes] They are included in Appendix A
3. If you ran experiments...
 - (a) Did you include the code, data, and instructions needed to reproduce the main experimental results (either in the supplemental material or as a URL)? [Yes] In Appendix C
 - (b) Did you specify all the training details (e.g., data splits, hyperparameters, how they were chosen)? [Yes] In Appendix C.
 - (c) Did you report error bars (e.g., with respect to the random seed after running experiments multiple times)? [Yes] We report standard deviations.
 - (d) Did you include the total amount of compute and the type of resources used (e.g., type of GPUs, internal cluster, or cloud provider)? [Yes] See Appendix C
4. If you are using existing assets (e.g., code, data, models) or curating/releasing new assets...
 - (a) If your work uses existing assets, did you cite the creators? [Yes]
 - (b) Did you mention the license of the assets? [N/A] We only use public datasets and code.
 - (c) Did you include any new assets either in the supplemental material or as a URL? [Yes] We include our code in the supplemental material.
 - (d) Did you discuss whether and how consent was obtained from people whose data you're using/curating? [N/A]
 - (e) Did you discuss whether the data you are using/curating contains personally identifiable information or offensive content? [N/A]
5. If you used crowdsourcing or conducted research with human subjects...
 - (a) Did you include the full text of instructions given to participants and screenshots, if applicable? [N/A]
 - (b) Did you describe any potential participant risks, with links to Institutional Review Board (IRB) approvals, if applicable? [N/A]
 - (c) Did you include the estimated hourly wage paid to participants and the total amount spent on participant compensation? [N/A]

Appendices

A Proofs

A.1 Proof of Theorem 1

Proof. We denote the perturbed node features as X' and change Equation (2) to the following equivalent form:

$$Z^{(k)} = \gamma^k g^k(F) Z^{(0)} S^k + \sum_{i=0}^{k-1} \gamma^i g^i(F) X' S^i.$$

Let $k \rightarrow \infty$, the first term becomes zero as $\gamma < 1$. We further decompose the above equation to $Z^{(k)} = \sum_{i=0}^{h-1} \gamma^i g^i(F) X S^i + \sum_{i=h}^{k-1} \gamma^i g^i(F) X S^i$. Since node p and q are h -hop apart, $S_{p,q}^i = 0$ when $i < h$. Then, we have $Z^{(k)} = \sum_{i=h}^{k-1} \gamma^i g^i(F) X' S^i$.

Let the perturbed features $X'_{:,p} = X_{:,p} + \Delta X_{:,p}$, we have $(X' S^i)_{:,q} = (X S^i)_{:,q} + \Delta X_{:,p} S_{p,q}^i$. Then we have the following:

$$\Delta Z_{:,q}^{(k)} = \sum_{i=h}^{k-1} \gamma^i g^i(F) (\Delta X_{:,p} S_{p,q}^i) \quad (14)$$

Apply the L2 norm on the change $\Delta Z_{:,q}^{(k)}$,

$$\|\Delta Z_{:,q}^{(k)}\| = \sum_{i=h}^{k-1} \gamma^i \|g^i(F) \Delta X_{:,p} S_{p,q}^i\| \quad (15)$$

$$\leq \left(\sum_{i=h}^{k-1} \gamma^i \right) \|g^h(F) \Delta X_{:,p} S_{p,q}^h\| \quad (16)$$

$$\leq \frac{\gamma^h - \gamma^k}{1 - \gamma} \|g^h(F) \Delta X_{:,p} S_{p,q}^h\| \quad (17)$$

The last inequality is derived by the sum of a geometric series.

As $k \rightarrow \infty$, $Z^* = \lim_{k \rightarrow \infty} Z^{(k)}$ and $\lim_{k \rightarrow \infty} \gamma^k = 0$. Then we have the following upper bound:

$$\|\Delta Z_{:,q}^*\| \leq \frac{\gamma^h}{1 - \gamma} \|g^h(F) \Delta X_{:,p} S_{p,q}^h\| \quad (18)$$

□

A.2 Proof of Corollary 1

Proof. Given the θ -effective range h , combining Definition 1 and Equation (3) in Theorem 1, we have $\theta < \Delta Z_{:,q}^* \leq \frac{\gamma^h}{1 - \gamma} \|g^h(F) \Delta X_{:,p} S_{p,q}^h\|$. Since $(1 - \gamma) > 0$, this is equivalent to $\gamma^h > (1 - \gamma)\theta$ and thus $h \ln \gamma > \ln((1 - \gamma)\theta)$. Since $\ln \gamma < 0$, we have that

$$h < \frac{\ln(\theta(1 - \gamma))}{\ln \gamma}. \quad (19)$$

Therefore, if node features $X_{:,p}$ of node p are perturbed, the perturbation can only affect the equilibrium of nodes which are up to $\frac{\ln(\theta(1 - \gamma))}{\ln \gamma}$ -hop away from p .

□

A.3 Proof of Theorem 2

Proof. For any matrix $M \in \mathbb{R}^{m_1 \times m_2}$, we define the vectorization of the matrix by $\text{vec}[M] \in \mathbb{R}^{m_1 m_2}$, and the Frobenius norm of the matrix by $\|M\|_F$. We define the map φ by $\varphi(Z) = \gamma g(F) Z S^m +$

$f(X, \mathcal{G})$. Recall that $Z \in \mathbb{R}^{h \times n}$. We want to show that the map φ is contraction. Using the property of the vectorization and the Kronecker product,

$$\text{vec}[\varphi(Z)] = \gamma \text{vec}[g(F)ZS^m] + \text{vec}[f(X, \mathcal{G})] = \gamma[(S^m)^\top \otimes g(F)] \text{vec}[Z] + \text{vec}[f(X, \mathcal{G})].$$

Therefore, for any $Z, Z' \in \mathbb{R}^{h \times n}$,

$$\begin{aligned} \|\varphi(Z) - \varphi(Z')\|_F &= \|\text{vec}[\varphi(Z)] - \text{vec}[\varphi(Z')]\|_2 \\ &= \|\gamma[(S^m)^\top \otimes g(F)](\text{vec}[Z] - \text{vec}[Z'])\|_2 \\ &\leq \gamma\|[(S^m)^\top \otimes g(F)]\|_2 \|\text{vec}[Z] - \text{vec}[Z']\|_2 \\ &= \gamma\|[(S^m)^\top]\|_2 \|g(F)\|_2 \|\text{vec}[Z] - \text{vec}[Z']\|_2 \\ &\leq \gamma\|Z - Z'\|_F. \end{aligned}$$

Since $\gamma \in [0, 1)$, this shows that φ is a contraction mapping on the metric space $(\mathbb{R}^{h \times n}, \hat{d})$ where $\hat{d}(Z, Z') = \|Z - Z'\|_F$. Thus, using the Banach fixed-point theorem, the desired statement of this theorem follows. \square

A.4 Proof of Theorem 3

We denote the perturbed node features as X' and change Equation (4) to the following equivalent form:

$$Z^{(k)} = \gamma^k g^k(F) Z^{(0)} S^{mk} + \sum_{i=0}^{k-1} \gamma^i g^i(F) X' S^{im}.$$

Following the similar procedure in the proof of Theorem 1, as $k \rightarrow \infty$ and $S_{p,q}^i = 0$ when $i < h$, we have $Z^{(k)} = \sum_{i=\lfloor h/m \rfloor}^{k-1} \gamma^i g^i(F) X' S^{im}$.

Let the perturbed features $X'_{:,p} = X_{:,p} + \Delta X_{:,p}$, we have $(X' S^i)_{:,q} = (X S^i)_{:,q} + \Delta X_{:,p} S_{p,q}^i$. Then we have the following:

$$\Delta Z_{:,q}^{(k)} = \sum_{i=\lfloor \frac{h}{m} \rfloor}^{k-1} \gamma^i g^i(F) (\Delta X_{:,p} S_{p,q}^{im}) \quad (20)$$

$$(21)$$

Apply the L2 norm on the change $\Delta Z_{:,q}^{(k)}$,

$$\|\Delta Z_{:,q}^{(k)}\| = \sum_{i=\lfloor \frac{h}{m} \rfloor}^{k-1} \gamma^i \|g^i(F) \Delta X_{:,p} S_{p,q}^{im}\| \quad (22)$$

$$\leq \frac{\gamma^{\frac{h}{m}} - \gamma^k}{1 - \gamma} \|g^{\frac{h}{m}}(F) \Delta X_{:,p} S_{p,q}^h\| \quad (23)$$

As $k \rightarrow \infty$, $Z^* = \lim_{k \rightarrow \infty} Z^{(k)}$ and $\lim_{k \rightarrow \infty} \gamma^k = 0$. Then we have the following upper bound:

$$\|\Delta Z_{:,q}^*\| \leq \frac{\gamma^{\frac{h}{m}}}{1 - \gamma} \|g^{\frac{h}{m}}(F) \Delta X_{:,p} S_{p,q}^h\| \quad (24)$$

A.5 Proof of Corollary 2

Proof. Similarly to the proof of Corollary 1 above, if h satisfies that $\frac{\gamma^{h/m}}{1-\gamma} > \theta$, then the numerical error θ does not dominate. Since $(1 - \gamma) > 0$ and $\ln \gamma < 0$, this is equivalent to

$$h < \frac{m \ln(\theta(1 - \gamma))}{\ln \gamma}. \quad (25)$$

Therefore, the change on node p 's features can affect the equilibrium of node q which is up to $\frac{m \ln(\theta(1-\gamma))}{\ln \gamma}$ -hop away from p . \square

A.6 Derivation of the gradients

Here, we provide the derivation of Equation (11) for obtaining gradients of trainable parameters with implicit differentiation. Using the chain rule, the gradients of trainable parameters can be computed by:

$$\frac{\partial \ell}{\partial (\cdot)} = \frac{\partial \ell}{\partial Z^*} \frac{\partial Z^*}{\partial (\cdot)}, \quad (26)$$

where (\cdot) denotes any trainable parameters within or before the implicit layer $Z^* = \varphi(Z^*, X, \mathcal{G})$. Note that $\frac{\partial \ell}{\partial (\cdot)}$ is directly handled by automatic differentiation (autodiff) packages, while $\frac{\partial Z^*}{\partial (\cdot)}$ cannot be directly obtained with autodiff since Z^* and (\cdot) are implicitly related.

By differentiating the both side of the fix-point equation, we can have:

$$\frac{\partial Z^*}{\partial (\cdot)} = \frac{\partial \varphi(Z^*, X, \mathcal{G})}{\partial Z^*} \frac{\partial Z^*(\cdot)}{\partial (\cdot)} + \frac{\partial \varphi(Z^*, X, \mathcal{G})}{\partial (\cdot)}, \quad (27)$$

where we use $Z^*(\cdot)$ to denote the case where we treat Z^* as an implicit function of variables we are differentiating with respect to (e.g., the parameters of φ) and Z^* alone to refer to the value of equilibrium.

By rearranging the above equation, we can obtain the explicit expression for $\frac{\partial Z^*}{\partial (\cdot)}$:

$$\frac{\partial Z^*}{\partial (\cdot)} = (I - J_\varphi(Z^*))^{-1} \frac{\partial \varphi(Z^*, X, \mathcal{G})}{\partial (\cdot)}, \quad (28)$$

where $J_\varphi(Z^*) = \frac{\partial \varphi(Z^*, X, \mathcal{G})}{\partial Z^*}$.

Combining Equation (28) and (26), we can have the following:

$$\frac{\partial \ell}{\partial (\cdot)} = \frac{\partial \ell}{\partial Z^*} (I - J_\varphi(Z^*))^{-1} \frac{\partial \varphi(Z^*, X, \mathcal{G})}{\partial (\cdot)}. \quad (29)$$

B Inefficiency of using higher γ

Using a large contraction factor γ usually make the process of finding the fixed-point more instable and difficult and it requires more iterations to find the fixed-point solution, which compromises the efficiency. We conduct the empirical experiments to verify this. We use EIGNN [20] with iterative solvers as the model on the chain dataset (as described in Sec 4). Table 5 demonstrates the training time of using different values of γ . We can see that when using $\gamma = 0.9$ can cost 2x training time compared with using $\gamma = 0.8$. Smaller γ empirically causes faster convergence to get the fixed-point solutions.

γ	0.6	0.8	0.9	0.95
Time per epoch	0.86s	1.65s	3.71s	3.95s
Total time	4596s	8267s	18580s	19916s

Table 5: Training time with different γ used in the iterative method.

Besides EIGNN, IGNN also faces instability in the training if it uses a large contraction factor. Different with Equation (2), IGNN projects the weight matrix W with a contraction factor κ onto a convex constraint set to ensure the convergence of iterative mapping. In their official implementation repo ², they mention that too large κ may cause the non-convergence of the equilibrium equation, which leads significant performance degradation. In the training log they provided ³, with $\kappa = 0.98$, we can see that the loss suddenly jump to more than 2000 from around 0.019 and the accuracy degrades from 0.96 to 0.39. This verifies again that a large contraction factor may cause instability during the training, although EIGNN and IGNN use different ways for contraction.

²<https://github.com/SwiftieH/IGNN/issues/3>

³https://github.com/SwiftieH/IGNN/files/7052441/PPI_output_log.txt

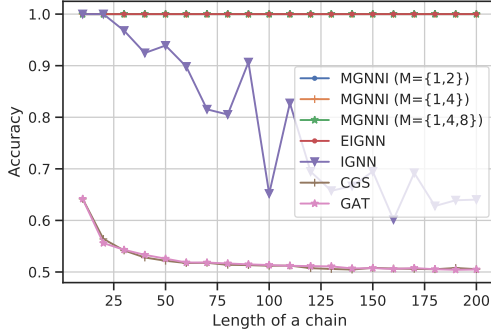


Figure 4: Averaged accuracies on Chains dataset: compare MGNNI to implicit and explicit GNNs.

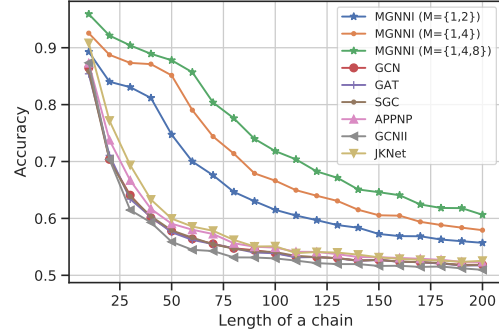


Figure 5: Averaged accuracies on color-counting dataset: compare MGNNI with explicit GNNs.

C More on Experiments

C.1 Synthetic experiments

Chains dataset The synthetic chain dataset is used in Gu et al. [13] and Liu et al. [20] to evaluate the ability of models to capture distant information. Chain dataset contains several chains directed from one end to the other with length l . The label information is only encoded as the node features in the starting end node of each chain. The nodes on the same chains share the same class label. The task is to classify nodes into different classes, which requires simply passing information from one end to the other end of a chain graph. We consider binary classification, 20 chains for each class, and l nodes in each chain. Then, the chain dataset has $40 \times l$ nodes. We randomly split the dataset for train/val/test as 5%/10%/85%.

In Figure 1 of Section 4, the starting end node is regarded as node p . We perturb the node features of starting node p by masking the features to all zeros. After that, we measure the L2 norm of the change in node q 's equilibrium as increasing the distance between node q and p to support our analysis.

Here, as in Liu et al. [20] and Gu et al. [13], we also provide the averaged results over 20 runs on the Chains dataset for comparison between MGNNI and other representative baselines in Figure 4. As we can see, MGNNI with different scale combinations can all achieve 100% accuracy as EIGNN, which indicates the superiority of capturing long-range dependencies. In contrast, IGNN has decreasing accuracies as the chain length increases. CGS has similar performance with GAT, which demonstrates the deficiency in capturing long-range information. We conjecture the reason is that CGS uses a single layer attention variant of graph network (GN) [6] as the input transformation which is a finite GNN as GAT. For simplicity, we omit more results of other explicit GNNs as those results can be provided by Liu et al. [20] in their Figure 1. Note that those explicit GNNs all generally perform worse than IGNN and EIGNN.

More results on color-counting dataset Besides the comparison between MGNNI and other implicit GNNs, we also compare MGNNI with explicit GNN models. Figure 5 shows that MGNNI with different scales consistently outperform all explicit GNNs, which confirms that MGNNI as an implicit GNN model has the better ability to capture long-range dependencies compared with explicit GNNs. Explicit GNN models still can achieve more than 85% accuracy when the chain length is 10. It is because that the test set are randomly sampled where some test nodes may be placed nearby the starting end node. However, the performance of explicit GNNs drops quickly as the chain length increases.

C.2 Node classification on real-world datasets

Dataset descriptions We first use 5 heterophilic graph datasets as in Pei et al. [23] to evaluate the capability of capturing long-range dependencies:

- **Chameleon and Squirrel:** these graphs are originally collected by Rozemberczki et al. [25], using the web pages in Wikipedia of the corresponding topic. Nodes represent web pages and edges are

hyper-links from a web page to another. The class labels are generated by Pei et al. [23]. There are 5 categories indicating the amount of the average monthly traffic of web pages.

- **Cornell, Texas, and Wisconsin:** these datasets contain the web-page graphs of the corresponding universities. Label classes indicate the category of web pages, where 5 classes are considered, i.e., student, faculty, course, project, and staff. These three datasets are collected by the CMU WebKB project⁴. The preprocessed version generated by Pei et al. [23] is used in our experiments.

To evaluate the model capacity on multi-label multi-graph inductive setting, we conduct the experiment on Protein-Protein Interaction (PPI) dataset. The dataset is originally collected from the Molecular Signatures Database [26] by Hamilton et al. [14]. PPI dataset has 24 graphs, where each graph represents a different human tissue. Each graph has nodes representing proteins and edges indicating interactions between proteins. Each node can have maximum 121 labels which represents gene ontology sets. We use the same data splits as in Hamilton et al. [14], i.e., 20 graphs for training, two graphs for testing, and two other graphs used for validation.

Experimental settings For heterophilic graphs, we compare MGNNI with 3 implicit GNNs (i.e., IGNN [13], EIGNN [20], and CGS [21]) and 8 explicit GNNs (i.e., Geom-GCN [23], SGC [28], GCN [17], GAT [27], APPNP [18], JKNet [30], GCNII [8], and H2GCN [34]). As we follow the exact same setting as in [20], we reuse their results of baselines, except CGS. For CGS and MGNNI, we conduct the experiments with 20 different runs and report the averaged accuracies with standard deviation.

For network architectures used in MGNNI on heterophilic graphs, we use two-layer MLP followed by the ReLU function as input features transformation $f(\cdot)$ and a linear map as the output transformation function (i.e., $f_o(X) = WX$). The hyperparameter search space is set as follows: multiscale set $M \{\{1,2\}, \{1,3\}, \{1,2,3\}\}$, weight decay $\{5e-6, 5e-4\}$, learning rate $\{0.01, 0.05, 0.1, 0.5\}$. We use $\gamma = 0.8$ for all scale modules and 0.5 as the dropout rate. The Adam optimizer [16] is used for optimization. For CGS, we use the suggested network architectures (i.e., a single layer attention variant of graph network (GN) [6] and the same number of hidden neurons as in CGS paper [21]). For other hyperparameter tuning, we optimize over learning rate $\{0.001, 0.005, 0.01, 0.05\}$, weight decay $\{5e-6, 5e-4\}$, and $\gamma \{0.5, 0.8\}$.

For PPI datasets, we use a 4-layer MLP directly after the multiscale propagation, while IGNN applies 4 MLPs between four consecutive IGNN layers. We set $\{1,2\}$ as the multiple scales in our propagation module, and use 0.001 as the learning rate. No dropout is used.

C.3 Graph classification on real-world datasets

Dataset descriptions We conduct experiments on 4 bioinformatics datasets (MUTAG, PTC, PROTEINS, NCI1) and 2 social-network datasets (IMDB-Binary and IMDB-Multi), following identical settings as in [31, 13]. MUTAG is a dataset having 188 graphs representing mutagenic aromatic and heteroaromatic nitro compounds with 7 discrete labels. PTC is a dataset of 344 chemical compounds reporting the carcinogenicity for male and female rats and it has 19 discrete labels. PROTEINS is a dataset where nodes are secondary structure elements (SSEs) and an edge between two nodes indicates they are neighbors in the amino-acid sequence or in 3D space. It has 3 discrete labels, representing sheet, helix or turn. NCI1 is a subset of balanced datasets of chemical compounds screened for ability to suppress or inhibit the growth of a panel of human tumor cell lines with 37 discrete labels and it is made publicly available by the National Cancer Institute (NCI).

IMDB-Binary and IMDB-Multi are social-network datasets, indicating movie collaborations. Each graph contains a ego-graph for each actor/actress, where nodes represent actors/actresses and edges connect two actors/actresses if they appear in the same movie. Labels are pre-specified genres of movies and each graph has the label corresponding to its genre. The task requires models to classify the genre.

Experimental settings We compare MGNNI with several representative baselines, including several explicit GNNs: Graph Convolution Network (GCN) [17], Deep Graph Convolutional Neural Network (DGCNN) [33], Fast and Deep Graph Neural Network (FDGNN) [10], and Graph Isomor-

⁴<http://www.cs.cmu.edu/webkb/>

phism Network (GIN) [31], and two other implicit GNNs: Implicit Graph Neural Network (IGNN) [13] and Convergent Graph Solver (CGS) [21].

Since we follow the same experimental settings as in [13, 31], we reuse the results of baselines from [13, 21], except EIGNN [20]. For the network architectures used in MGNNI for graph classification, we use three-layer MLP followed the ReLU function as input feature transformation $f(\cdot)$. After the multiscale propagation with attention mechanism, we use the sum-pooling aggregator to obtain the graph representations. A linear map is used as the output transformation function (i.e., $f_o(X_g) = WX_g$). We set the number of hidden state as 32, $y = 0.8$ for all scale modules. The search space for the other hyperparameters is set as follows: multiscale set $M \{\{1,2\}, \{1,3\}\}$, weight decay $\{0, 5e-6\}$, and learning rate $\{0.001, 0.01\}$. The Adam optimizer [16] is used for optimization. For EIGNN, after their implicit layer, we use a 3-layer MLP with ReLU activation followed the sum-pooling layer to obtain the graph representations. A 2-layer MLP is used for generating the final predictions. γ is set to 0.8 and other hyperparameters (learning rate and weight decay) are tuned over the same search space.

C.4 Efficiency Comparison

Here, we provide the efficiency comparison among IGNN, EIGNN, and MGNNI on PPI dataset. Table 6 demonstrates the training time per epoch and the total pre-processing time of different models. We can see that IGNN requires around 30s for training an epoch, while EIGNN and MGNNI requires only around 2s for an epoch. The reason of inefficiency in IGNN is that IGNN requires 4 implicit layers sequentially stacked, which means that every iterative solver needs to wait the fixed-point solution provided by the previous iterative solver for solving its own solution. In contrast, MGNNI have parallel equilibrium layers with different scales, where each equilibrium layer can get the fixed-point solution simultaneously. Thus, the training time per epoch of MGNNI is similar with that of EIGNN which only has one implicit layer. Additionally, MGNNI does not require pre-processing time to conduct eigendecomposition of the adjacency S as EIGNN which may be costly for large graphs.

Table 6: Training time per epoch on PPI.

Method	Train Time	Pre-process
IGNN	32.7s	N.A.
EIGNN	2.3s	45s
MGNNI	2.6s	N.A.

C.5 The effect of the attention mechanism

To quantitatively investigate the effect of the attention mechanism in MGNNI, we conduct additional experiments by removing the attention mechanism and instead use average pooling for fusing information from multiple scales. The experimental results are provided in Table 7. We can see that, if we replace the attention mechanism with average pooling, the performance would drop. It verifies the effectiveness of our attention mechanism, which is also demonstrated in Figure 3 and its corresponding explanations in Section 6.3.

Table 7: Performance of different scales.

Scales	PPI	Chameleon	Texas
(wo/ att) {1,2}	98.35	61.46	81.35
(w/ att) {1,2}	94.62	58.24	82.97
(wo/ att) {1,2}	98.67	63.93	83.24
(w/ att) {1,2}	98.74	63.75	84.86